VARIABILITY IN MARTIAN CO AS OBSERVED BY NOMAD-SO FROM FIRST YEAR OF TGO OPERATION.

Ashimananda Modak, *(ashim@iaa.es)*, **M. A. López-Valverde, A. Brines, A. Stolzenbach, B. Funke, F. González-Galindo,** *Instituto de Astrofísica de Andalucia, Granada, Spain*, **S. Aoki,** *Belgian Royal Institute for Space Aeronomy, Brussels, Belgium*, *Japan Aerospace Exploration Agency (JAXA), Japan*, **I. Thomas,** *Belgian Royal Institute for Space Aeronomy, Brussels, Belgium*, **G. Liuzzi,** *NASA Goddard Space Flight Center, USA*, **G. Villanueva,** *NASA Goddard Space Flight Center, USA*, **J. Erwin,** *Belgian Royal Institute for Space Aeronomy, Brussels, Belgium*, **J. J. Lopez-Moreno,** *Instituto de Astrofísica de Andalucia, Granada, Spain*, **N. Yoshida,** *Graduate School of Science, Tohoku University, Sendai, Japan*, **U. Grabowski,** *Karlsruhe Institute of Technology, Institute of Meteorology and Climate Research, Karlsruhe, Germany*, **F. Forget,** *Laboratoire de Météorologie Dynamique, IPSL, Paris, France*, **F. Daerden,** *Belgian Royal Institute for Space Aeronomy, Brussels, Belgium*, **B. Ristic,** *Belgian Royal Institute for Space Aeronomy, Brussels, Belgium*, **G. Bellucci,** *Institute for Space Astrophysics and Planetology, Italy*, **M. Patel,** *Open University, Milton Keynes, UK*, **L. Trompet,** *Belgian Royal Institute for Space Aeronomy, Brussels, Belgium*, **A.C. Vandaele,** *Belgian Royal Institute for Space Aeronomy, Brussels, Belgium*.

Introduction

Mars' atmosphere is primarily a CO_2 atmosphere with an amount of $\sim 95\%$ and the rest of the $\sim 5\%$ of the atmospheric mass is composed of trace gases such as O_2, H_2, CO, H_2O, O_3, OH, HO_2, etc. During the daytime exposure to the sunlight, CO_2 breaks into CO and O and is recycled via a chemical reaction of CO with OH [6]. Like any other chemically active trace species, the measurement of CO is important to characterize and understand the chemical processes in the atmosphere. In addition, CO is also important for being a dynamical tracer due to its long lifetime [4].

Columnar measurements of CO have been carried out by few spaceborne instruments such as CRISM (Compact Reconnaissance Imaging Spectrometer for Mars) [10], PFS (Planetary Fourier Spectroscopy) [1], OMEGA (Observatoire pour la Minéralogie, l'Eau, les Glaces et l'Activité) [2], and more recently by the LNO(Limb Nadir and solar Occultation) channel of the NOMAD(Nadir and Occultation for MArs Disovery instrument) instrument on board TGO (Trace Gas Orbiter)[11]. The columnar measurements revealed the seasonal and latitudinal distribution of CO. One of the important results confirmed by these studies is the increase in the relative abundance of CO, or volume mixing ratio (VMR), during the polar winter. This is resulting from the known seasonal change in CO_2, the main atmospheric species at Mars. These measurements also established a global average of 800 ppm for CO mixing ratios.

However, the observations of vertical profiles of CO have become possible in a systematic manner thanks for the TGO Exomars 2016 mission. We report here new results of CO vertical profiles obtained for the first tie from the SO channel of the NOMAD instrument on board TGO. Largely based on a recent work submitted to JGR-Planets [8], this study covers the first year of TGO science operations, which extended for the last two seasons of MY34.

Data Processing and Retrieval

The NOMAD instrument is a suite of three spectrometers SO, LNO and UVIS (ultraviolet and visible spectrometer). Two of them SO and LNO operate in the infrared and the third one, UVIS, operates in the UV [13]. Our objective here is to retrieve carbon monoxide from the SO observations. The SO spectrometer integrates an echelle grating in littrow configuration with an Acousto Optical Tunable Filter (AOTF) for selecting the desired diffraction orders [9]. The NOMAD-SO channel covers a wavelength range of 2.3 - 4.3 μm. In this spectral range, five different diffraction orders, internally named as 186 - 191, contain strong CO lines and are suitable for CO retrievals. We only used order 190 in this work.

The SO measurements are level 1 transmittance data shown in the left panel of Figure 1. The calibrated transmittances suffer from diverse imprecissions and systematics, in particular from small spectral shifts and broad spectral bendings. We developed a pre-processing or cleaning method to correct for spectral shifts and bending effects, based on precise line-by-line simulations including a climatological atmospheric state and incorporating the SO instrumental response. This preproccessing is applied to small regions, or spectral microwindows (MW), within each diffraction order. The bending is corrected in each MW while the spectral shift correction is assumed to be linear across the order and therefore requires several MWs. In order 190 we used 4 MWs. Our line-by-line calculations were performed with the KOPRA model (Karlsruhe Optimized and Precise Radiative transfer Algorithm) [12].

The cleaned spectra are used as inputs in the inversion. The inversion is performed with a retrieval control program (RCP) which uses Levenberg-Marquardt minimization method to solve for CO using the forward model KOPRA iteratively [5]. The *a-priori* temperature and pressure are are not obtained from a climatology but from a previous retrieval of the same Nomad/SO

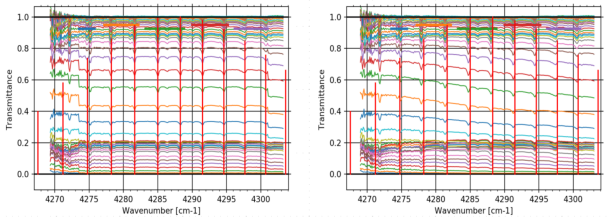

Figure 1: Right panel: Level 1 calibrated transmittance spectra from 1 scan. Each spectrum is shown with a different color and corresponds to a different tangent altitude. Vertical lines indicate CO line positions from Hitran 2016, for reference. It can appreciate a residual spectral bending and a spectral shift. Left panel: Same transmittances after the cleaning (not applied to the edges of the order).

scan performed by our team [7]. The *a-priori* The *a-priori* CO profile is taken from the LMD-GCM (Mars Global Climate Model developed at the Laboratoire de Météorologie Dynamique) simulations.

An example retrieval is shown in the Figure 2 together with few diagnostic plots. In the Figure four panels, from the left, show CO, averaging kernel, percentage error and vertical resolution respectively. The averaging kernel describes the mapping of the measurements onto the retrieval grid and the vertical resolution is described by FWHM (Full Width at Half Maxima) of the averaging kernel. The errors of the retrievals are typically within 10 - 15% and the vertical resolutions are better than 5km below the altitude 80km.

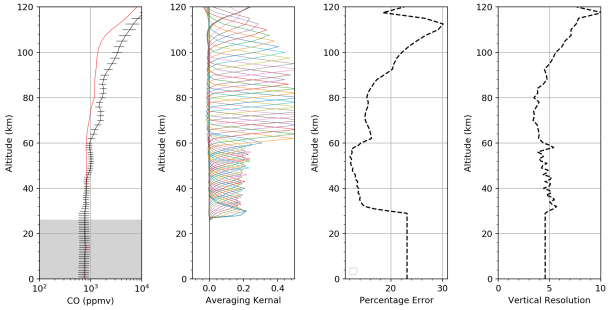

Figure 2: Retrieved CO VMR profile for one particular scan (left panel) and three profile's diagnostics: averaging kernel rows, retrieval error in percentage, and vertical resolution in km. The data below 25 km is ignored due to the large dust opacity.

Temperature Dependence of the Retrievals

One of the main challenges for the CO retrieval is its dependence on temperature and pressure. To illustrate this dependence, Figure3 shows results of two retrievals,

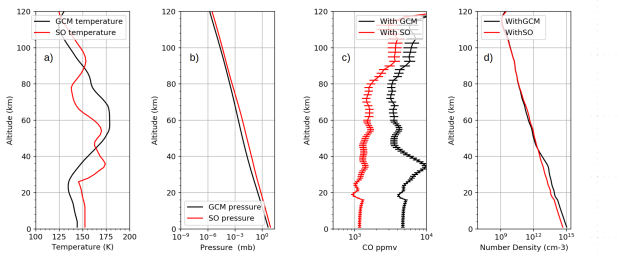

Figure 3: The effect of the reference atmosphere on the retrieved CO. First and second panels from left: reference temperature and pressure from LMD-GCM and SO retrieval respectively. Third and fourth panels: the volume mixing ratio and number density of CO retrived with temperature and pressure from GCM (black) and SO (red).

one with *a-priori* temperature and pressure from GCM (plotted in black) and another with *a-priori* temperature and pressure retrieved from a different diffraction order(plotted in red)[7]. The retrieved VMR and number density of CO with SO T/P are shown in red curves in the panels c and d while those with GCM T/P are in black.

The VMR values retrieved using GCM T/P are notably higher than the values retrieved with retrieved temperature and pressures. Both pressure and temperature affect the inversion of CO. The VMR is affected by both while the absolute CO (panel d) is possibly affected most by temperature. In both cases, retrieved absolute number density values are similar above 40km but below, the values differ. Below 40km, lower values of CO density are retrieved for the warmer, i.e., the SO temperature.

CO Vertical Profiles and Variability

Here we present, briefly, the results obtained in the retrieval from the SO observation of order 190. Due to the dependence on temperature and pressure, we only have attempted to retrieve CO from scans with simultaneous temperature retrievals. These were performed by our team previously, from NOMAD/SO data in order 149. There are 275 such scans for MY34, among which 200 were successful. All the retrieved profiles are shown in panels c and d of Figure 4. Panel c is corresponding to the Northern hemisphere and d to the Southern. Panels a and b show the location of the profiles in c and d respectively.

CO is a long-lived species affected by both photochemistry and long range transport. The photochemical production of CO occurs at high altitudes while its chemical loses are most effective at low altitudes. We observe increasing CO VMR with altitudes as a general trend in our retrieved CO VMR vertical profiles. Particularly, high values and large gradients are observed in the alti-

tudes above 60km.

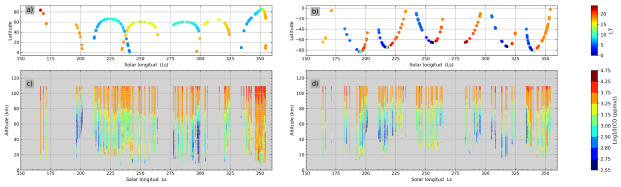

Figure 4: All the retrieved CO profiles plotted against season and altitude in panel c for the Northern hemisphere and in panel d for the Southern hemisphere. The panels a and b respectively, indicate the latitude and season of each profile

The dataset extends from April 2018 to March 2019, i.e., Northern Autumn and Winter MY34, including the MY34 global dust storm (GDS). In the work by [8] we study the variability in CO in detail. We will highlight some results here, like the CO at high altitudes. This is described by the iso-contour indicating a value $log_{10}(\mathrm{CO(in\ VMR)}) = 3.5$ (orange color). The high altitude CO seems to downwell and reaches, successively, to low altitudes over Northern hemisphere (panel c, Figure 4). The downwelling reaches about 60km during the Southern summer at Ls $\sim 275^{\circ}$. While over the Southern hemisphere, this iso-contour seems to retreat towards altitudes higher than 80km. However, the downwelling of CO seems to increase during the end of the year over both hemispheres.

The variability of the CO VMR below 60km altogether reflects a different seasonality. During GDS, the CO of this region depletes due to warming of the atmosphere which in turn facilitates the atmosphere to hold more water vapor. The increase in the water vapor produces an increase in OH radicals which is normally the primary photochemical destruction of CO at these altitudes. On contrary, during the decay phase of the GDS (Ls $= 210^{\circ} - 225^{\circ}$), in the presence of high optical depth an increase in the low altitude $\sim$ 20km CO is observed. This increase is puzzling, when combined with the CO behavior during the peak of the GDS. It suggests that the photochemical destruction by OH and the H_2O photolysis are not the primary sources of CO loses, or that their effects are very non-linear with the dust opacity, or that different processes affecting CO are at work during the peak and decay phases of the GDS.

A depletion in the CO VMR, is again observed during the Southern summer over both the hemispheres. Over the Northern hemisphere, the depletion can be observed (Figure 4) in the period Ls $= 275^{\circ} - 300^{\circ}$ while over Southern hemisphere it extends till Ls $= 325^{\circ}$. During the Southern summer the well known phenomena of polar cap melting occurs which releases the trapped CO_2 and water vapor into the atmosphere. CO being a long-lived trace species may respond to both the causes.

The effect of Southern summer on CO distribution reduces and a general increase in VMR values of all the observed profiles found after Ls $= 325^{\circ}$. Over the Northern hemisphere, for this period, most of the profiles are located in the high latitudes and for these profiles, high CO values are retrieved for all the altitudes. However, over the Southern hemisphere, though the high values of CO are retrieved, a latitudinal gradient is also visible from the Figure 4.

Figure 5 shows the latitudinal variation for two selected periods corresponding to the onset of the GDS and to the Southern summer. The above panels a and b show the latitudinal distribution of the CO profiles and the panels c and d show the colocated GCM-simulated values. During the onset of the GDS, Martian dynamics is dominated by two Hadley cells extending from the equator to the high latitudes in both the hemispheres. The effect of the hemispheric Hadley circulation can be seen clearly in the CO distribution of LMD-GCM as well as in the observation. The increase in the low altitude CO over the high Southern latitudes (Figure 4) is due to this effect.

Another interesting result can be observed near the summer solstice season, regarding the latitudinal variation of CO. It is the clear pattern of the global Hadly cell typical of the dynamical regime of this period. The global Hadley cell [3] seems to extend from the Southern latitudes towards the Northern latitudes and downwells near the Lat $= 60^{\circ}$.

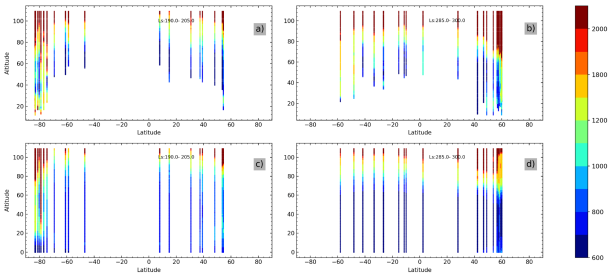

Figure 5: Latitudinal distribution of the CO profiles for the periods as indicated in the panels. The above panels (a and b) show the distribution of the retrieved CO and the below panels (c and d) show the corresponding distribution of CO profiles simulated by GCM. The color bar indicates the VMR values of CO.

Acknowledgments

The IAA/CSIC team acknowledges financial support from the State Agency for Research of the Spanish MCI through the "Center of Excellence Severe Ochoa" award (DEV-2017-0709) and funding by grant PGC2018-101836-B-100 (MCI/AEI/FEDER, EU). This project acknowledges funding by the Belgian Science Policy Office

(BELLS), with the financial and contractual coordination by the ESAU Prod ex Office (PEA 4000103401, 4000121493) as well as by UK Space Agency through grants ST/V002295/1, ST/V005332/1 and ST/S00145X/1 and Italian Space Agency through grant 2018-2-HHS.0. US investigators were supported by the National Aeronautics and Space Administration.

References

[1] J. Bouche, S. Bauduin, M. Giuranna, S. Robert, S. Aoki, A. C. Vandaele, J. T. Erwin, F. Daerden, P. Wolkenberg, and P.-F. Coheur. Retrieval and characterization of carbon monoxide (co) vertical profiles in the martian atmosphere from observations of pfs/mex. *Journal of Quantitative Spectroscopy and Radiative Transfer*, 238:106498, 2019.

[2] T. Encrenaz, T. Fouchet, R. Melchiorri, P. Drossart, B. Gondet, Y. Langevin, J.-P. Bibring, F. Forget, and B. Bézard. Seasonal variations of the Martian CO over Hellas as observed by OMEGA/Mars Express. *Astronomy & Astrophysics*, 459(1):265–270, 2006.

[3] F. Forget, F. Hourdin, R. Fournier, C. Hourdin, O. Talagrand, M. Collins, S. R. Lewis, P. L. Read, and J.-P. Huot. Improved general circulation models of the Martian atmosphere from the surface to above 80 km. *Journal of Geophysical Research: Planets*, 104(E10):24155–24175, 1999.

[4] F. González-Galindo, M. López-Valverde, M. Angelats i Coll, and F. Forget. Extension of a Martian general circulation model to thermospheric altitudes: UV heating and photochemical models. *Journal of Geophysical Research: Planets*, 110(E9), 2005.

[5] Á. A. Jurado Navarro et al. Retrieval of CO2 and collisional parameters from the mipas spectra in the earth atmosphere. 2016.

[6] V. A. Krasnopolsky. *Photochemistry of the Atmospheres of Mars and Venus*, volume 13. Springer Science & Business Media, 2013.

[7] M.-A. López-Valverde, B. Funke, A. Brines, A. Stolzenbach, A. Modak, B. Hill, F. GonzÃlez-Galindo, I. Thomas, L. Trompet, S. Aoki, G. Villanueva, G. Liuzzi, J. Erwin, A.-C. Vandaele, U. Grabowski, F. Forget, J. J. L. Moreno, J. Rodriguez, B. Ristic, F. Daerden, G. Bellucci, and M. Patel. Martian atmospheric temperature and density profiles 2 during the 1st year of NOMAD/TGO solar occultation 3 measurements. *JGR-submitted*, 2022.

[8] A. Modak, M.-A. López-Valverde, B. Funke, A. Brines, A. Stolzenbach, F. Gonzalez-Galindo, et al. Retrieval of martian atmospheric co vertical profiles from the first year of NOMAD/TGO solar occultation observations. *JGR-submitted*, 2022.

[9] E. Neefs, A. C. Vandaele, R. Drummond, I. R. Thomas, S. Berkenbosch, R. Clairquin, S. Delanoye, B. Ristic, J. Maes, S. Bonnewijn, et al. NOMAD spectrometer on the exoMars trace gas orbiter mission: part 1 - design, manufacturing and testing of the infrared channels. *Applied optics*, 54(28):8494–8520, 2015.

[10] M. D. Smith, F. Daerden, L. Neary, and A. Khayat. The climatology of carbon monoxide and water vapor on Mars as observed by CRISM and modeled by the gem-Mars general circulation model. *Icarus*, 301:117–131, 2018.

[11] M. D. Smith, F. Daerden, L. Neary, A. S. Khayat, J. A. Holmes, M. R. Patel, G. Villanueva, G. Liuzzi, I. R. Thomas, B. Ristic, et al. The climatology of carbon monoxide on Mars as observed by NOMAD nadir-geometry observations. *Icarus*, 362:114404, 2021.

[12] G. P. Stiller. The karlsruhe optimized and precise radiative transfer algorithm (KOPRA). 2000.

[13] A. C. Vandaele, J.-J. Lopez-Moreno, M. R. Patel, G. Bellucci, F. Daerden, B. Ristic, S. Robert, I. Thomas, V. Wilquet, M. Allen, et al. NOMAD, an integrated suite of three spectrometers for the exoMars trace gas mission: Technical description, science objectives and expected performance. *Space Science Reviews*, 214(5):1–47, 2018.